Switching Speed Analysis of MOSFET-Based Absorber Integrated Antenna for 5G/WiMAX/WLAN

Elliot O. Omoru and Viranjay M. Srivastava*
Department of Electronic Engineering, Howard College, University of KwaZulu-Natal, South Africa;
Email: omoruelliot@ieee.org, viranjay@ieee.org
*Correspondence: viranjay@ieee.org

***Abstract*—A block-by-block performance analysis of a novel Metal Oxide Semiconductor Field Effect Transistor (MOSFET)-based absorber antenna has been presented. The proposed integrated antenna is a solution to the negative effect of impedance mismatch between the power amplifier and antenna in the front end of communication systems. The clockwise diode base quasi circulator device used in the proposed design has been observed to have an insertion loss (S_{21} and S_{32}) of *7 dB* and *9.2 dB*, respectively, with a return loss (S_{22}) of *2.8 dB*. The MOSFET-based absorber presented an insertion loss, return loss, and absorption efficiency *of 2.75 dB, 3.3 dB,* and > *90%*, respectively. The switching speed for the proposed MOSFET-based absorber antenna model has been observed as *0.15 ns*.**

***Keywords*—absorber, antenna, pulse generator, circulator, solid-state electronics**

I. Introduction

Various transmit and receive front-end systems benefit from active integrated antennas because they can minimize the size, weight, and cost. This antenna device combines components like transistors with antenna elements to offer oscillation and amplification capabilities, thus allowing sophisticated devices [1]. Telecommunication systems, Radio Frequency Identification (RFID) tags, radio-sensors radiating systems for automobile and radar applications, and high-impedance nano-scale devices are using these antenna types [2, 3]. The Active Integrated Antenna (AIA) is an antenna with integrated signal-processing and wave-processing capabilities [3]. A typical AIA comprises planar antennas like dipoles, microstrip patches, bowties, or slot antennas, as well as active components like Gunn diodes or three-terminal components to create an active circuit. Active integrated antennas may considerably improve the performance of wireless communication systems, especially in the 5G era, where wireless equipment that will enable new 5G communication applications must be capable of handling large data rates [4]. Several antenna-integrated devices exist, including power amplifiers and integrated antennas, which have already in [5].

Manuscript received July 14, 2022; revised October 11, 2022; accepted January 22, 2023.

Some are antennas with active components that give oscillation function [6], antenna integrated with a low noise amplifier [7], voltage-controlled oscillators antennas [8], filtering antenna [9], antennas with injection-locking [10], antennas with oscillators that can switch bands [11], rectifier antenna [12], and antennas with switchable radiation patterns [13]. The antenna integration process entails numerous independent processes that often do not overlap in one design flow, but this technique includes all of them and provides reciprocal advantages for all components.

The rectifier antenna (rectenna) is remarkably popular due to its application in energy harvesting. This integrated antenna device captures ambient wireless electromagnetic energy via an antenna connected to rectifying diodes, which transform the received energy into Direct Current (DC) [12, 13]. They have a virtually infinite lifespan and are non-polluting, two significant benefits of batteries. Different design methodology has been adopted for this type of antenna. In [14], a flexible *50 m* thick co-planar waveguide rectenna filament and a spray-coated supercapacitor were combined to create a "e-textile" energy supply module. The meandering antenna maintains an S_{11} *6 dB* inside the fabric, outside of it, and when was observed to have a gain of *2.3 dBi* gain. The rectifier has an *80 %* peak RF-DC efficiency across *a 4.5 kΩ* load and a *1.8 V* open-circuit voltage from *-7 dBm*. The combined module has an end-to-end efficiency of *38 %* at *1.8 m* from the transmitter. The rectenna harvests *4 mJ* from approximately *16.6 W/cm*^{2} power densities in *32 s* with an on-body efficiency of *4.8 %*, accounting for in-body losses and transient shadowing. The researchers came to the conclusion that e-textile rectennas are the most effective way to power wearables at *W/cm* ^{2} power density.

Also, Muhammad *et al.* [15] have presented a Global System for Mobile communication (GSM) 900 and 1800 long-range dual-band rectenna for harvesting ambient RF energy. In this design, using a dual-band Impedance Matching Network (IMN) reduces the rectenna circuit complexity, which helps to improve the harvester's RF-to-dc power conversion efficiency. At *0.9 GHz* and *1.8 GHz*, the proposed device produced a peak RF-to-dc power conversion efficiency of *12.93%* and *8 %*, respectively, with an input power of *30 dBm*. The output dc voltage of the RF harvester ambiance measurement was *0.374 V*. Using a low-powered evaluation module, the circuit generates *0.747 V*. As a result, the proposed rectenna's

energy management may be utilized to power several low-powered devices using the gathered ambient RF energy.

In recent years, the amplifier-type active antenna has been one of the research's key concerns. This type of amplifier antenna has existed in the form of low noise amplifier antenna or power amplifier antenna for receiving and transmitting antenna, respectively [16]. Antenna and Low-Noise Amplifier (LNA) and antenna Power Amplifier (PA) co-design is a possible way of making microwave or millimeter-wave (mmWave) receiver and transmitter systems more sensitive. In order to reduce extra noise contributions, the co-design method for the low noise amplifier antenna presupposes a mutually advantageous design process for the antenna and LNA. To enhance the performance of the system, antenna design should take into account the ultimate output impedance Z_{opt} of the LNA employed in the co-design [17]. This is necessary because when a new cascade is introduced, the amplifier input impedance may shift, affecting the co-design system's performance. Also, because LNA does not have a standard impedance matching network in the co-design method, the antenna reflection coefficient must offer the ideal impedance for the amplifier noise-gain trade-off.

Rusdiyanto and Zulkifli [18], developed a low noise amplifier antenna in the Global Positioning System (GPS) band. The single passive antenna and low noise amplifier that make up the antenna integrated LNA were designed and tested using electronic device simulator. The observed gain for this LNA is *14.77 dBi*, but the simulation indicates a gain of *28.4 dBi*. The antenna features circular polarization with an axial ratio of less than *3 dB* in both simulated and measured findings, which are *1.58 dB* and *1.21 dB*, respectively.

On the power amplifier side, active devices and their associated biasing and matching circuits are directly integrated with the antenna, and the selection of an antenna type affects the design architecture and system performance. Other vital factors to consider when designing a power amplifier integrated with an antenna are the operation class of the power amplifier and heat dissipation inside the device. Several topologies for antennas are combined with power amplifiers [19].

Demirel et al. [20] designed a power amplifier antenna using metal oxide semiconductor technology. This design eliminated the need for a matching network between the power amplifier and the transmitter. After a complete analysis, it was observed that there was a reduction in transmission loss, improved efficiency. The differential Power amplifier presented a maximum output power of *17 dBm* at *79 GHz*. The supplied voltage of the chip was *1.8 V* using *300 mA* current with a gain of *–14 dB*. The antenna and PA have respective sizes of *0.7 mm*^{2} and *0.75 mm*^{2}. A cooperative design approach for a co-integrated antenna and PA was presented in reference [21]. This design uses a high-efficiency Doherty Power Amplifier (DPA) architecture with a band-pass RF filter. A *9 %* fractional bandwidth (*300 MHz*) with a Power Added Efficiency (PAE) at the *6 dB* backed-off power level that varies between *50 %* and *55 %* was attained after the simulation experiment. Between *48 %* and *53 %*, the efficiency levels observed were a little lower. Due to the radiating element's distributed and balanced multi-port feeding architecture, the antenna pattern variation does not exceed *0.1 dB* as the output power declines from its maximum. This combination of enhanced efficiency bandwidth and improved radiation pattern stability significantly improved over older antenna-integrated DPA systems.

Also, the design presented an increased insertion loss of approximately *1.5 dB*, the projected performance was expected at S_{11}*<-18 dB*. In [22] it contains similar research on integrated designs. However, some of these co-designed integrated PA antenna arrangements failed to take into account the detrimental impacts of antenna and PA mismatches.

A block-by-block performance analysis of a novel MOSFET-based absorbing antenna design of *Omoru and Srivastava* [23] have presented and analyzed using antenna performance parameters. The suggested antenna's MOSFET terminal's rectified reflected power may be boosted and utilized for low-power activities inside the RF front-end system.

This paper has been organized as follows. Section II presents an overview of the proposed MOSFET-based absorber integrated antenna. Section III shows the mathematical modeling for active 3 port diode base circulator. Section IV presents a block-by-block performance analysis of the proposed MOSFET-based absorber antenna. Also, in this session, the switching speed of the MOSFET base absorber antenna is analyzed. Finally, section V concludes the work and recommends future aspects.

II. Overview of Proposed MOSFET- Based Absorber Integrated Antenna Design

Four design stages have been adopted to realize a fully parameterized circuit model of the proposed MOSFET-based absorber integrated antenna. Stage one involves the design of a double-material cylindrical patch antenna (DMS CSPA). The technique used for this antenna design has been observed to provide increased bandwidth. Also, it is a solution to the problem of dimensional inaccuracy during the fabrication of a microstrip patch antenna [23]. Stage two involves the design of a diode-based active 3 port circulator. Stage three involves the MOSFET-based absorber design. Finally, integration of designed devices from stage one through stage three.

The author's previous work presented various views and basics of adopted modeling for cylindrical surrounding patch antenna used in the design [24, 25]. To extend that research, the proposed MOSFET-based absorber antenna designs antenna dimensions are shown in ref. [24].

The MOSFET based antenna employs a distinct quasi-circulator model based on diodes. Using a unilateral power divider/combiner, the features of a 3-port active diode base quasi circulator, and adopted modeling of a MOSFET base absorber, an example of a schematic is shown in Fig. 1. To realize the fully parameterized MOSFET base absorber antenna in Fig. 2, port-2 of the circulator is linked to the DMS CSPA, while port-3 of the circulator is connected to

the MOSFET-based absorber. To test these combined devices (double material cylindrical patch antenna, 3 port active circulator, and MOSFET based absorber), the circulator's port-1 receives the excitation signal supplied by the pulse generator [25].

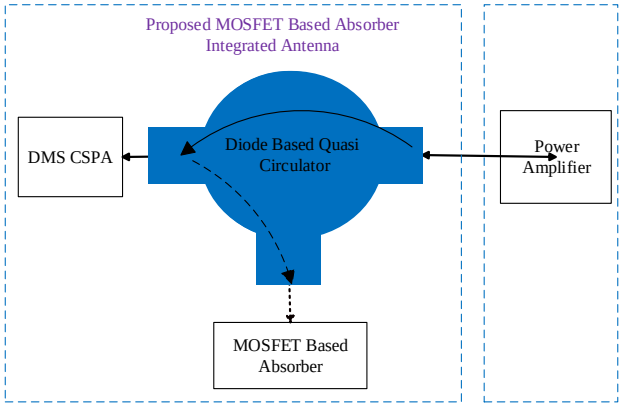

Figure 1. Proposed MOSFET base absorber antenna block diagram.

TABLE I. TERMINAL VALUES

Terminal	Voltage *(mV)*	Current *(mA)*
Source (P11)	0	-3.6
Drain(P10)	466	3.6

As seen in Fig. 2, if the conditions $I_S \leq I_D$ (current at p10 less than or equal to current at p11) and $V_{DS} = 0$ (voltage at p10 equal to 0) are met, the MOSFET in the antenna is considered to have accomplished its role of absorbing reflected signal from the antenna.

The drain current and voltage of the MOSFET are also noted and shown in Table I following the execution of a transient simulation on the suggested MOSFET-based absorber antenna design. It demonstrates that the proposed device satisfies the requirement for MOSFET absorption (source voltage is zero and source current is negative relative to drain current, implying a requirement of $I_S \leq I_D$).

III. MATHEMATICAL MODELLING OF 3 PORT DIODE-BASED QUASI CIRCULATOR

There are several microwave devices that are realized using a three-port network. To analyze this type of device, it is necessary to understand the s parameters and properties [26]. The operating condition of any three-port network is important in determining the type of microwave device. The first condition is to determine if it is a matched network. The second condition is to determine if the device is reciprocal or non-reciprocal, and lastly, check if the device is lossy or lossless. However, it is critical for these three conditions to be satisfied for a three-port microwave device [27].

For a three-port network, the matching condition is: $S_{11} = S_{22} = S_{33} = 0$. Also, for a three-port network, the condition for reciprocity is: $S_{ij} = S_{ji}$, for $j \neq i$ meaning $S_{12} = S_{21}$, $S_{13} = S_{31}$. Applying these two conditions, the S matrix becomes:

$$[s] = \begin{bmatrix} 0 & s_{12} & s_{13} \\ s_{12} & 0 & s_{23} \\ s_{13} & s_{23} & 0 \end{bmatrix}$$

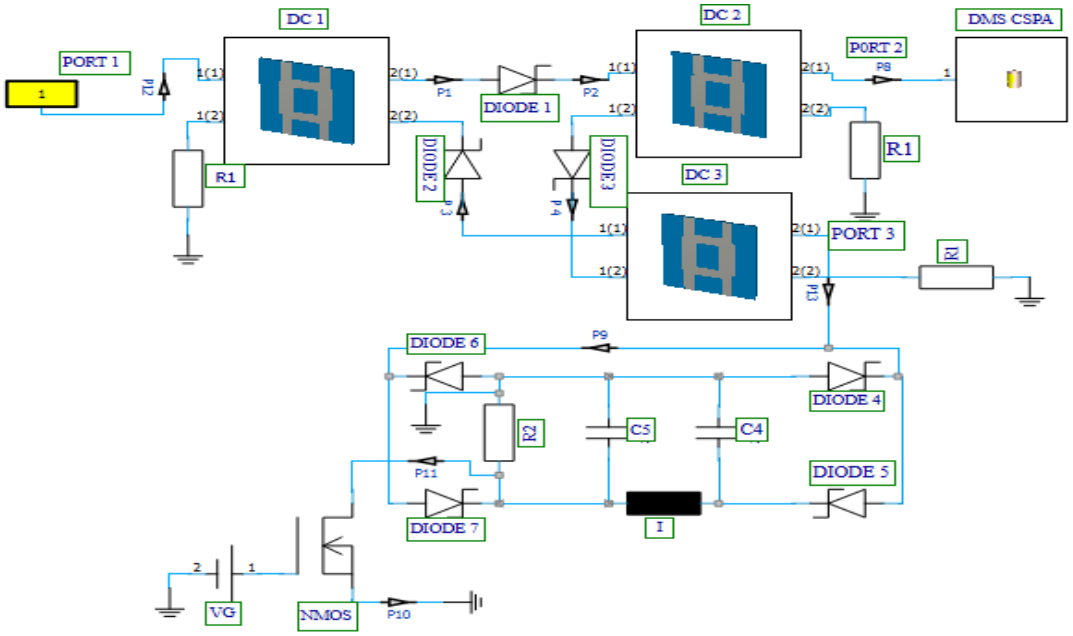

Figure 2. MOSFET-based absorber antenna design [25].

A lossless condition can be applied by taking the conjugate of the S-matrix derived from the matching condition and condition combination for reciprocity. First, consider the unitary case where the summation of the square of any column is equal to 1:

$$Column\ 1 = |s_{12}|^2 + |s_{13}|^2 = 1 \quad (1a)$$

$$Column\ 2 = |s_{12}|^2 + |s_{23}|^2 = 1 \quad (1b)$$

$$Column\ 1 = \left|s_{13}\right|^2 + \left|s_{23}\right|^2 = 1 \quad (1c)$$

Now, for a lossless condition:

$$S_{13}^{*} \times S_{23} = 0 \quad (2a)$$

$$S_{12} \times S_{13}^{*} = 0 \quad (2b)$$

$$S_{12} \times S_{23}^{*} = 0 \quad (2c)$$

where S_{I3}^{*}, and S_{23}^{*} represent conjugates of S_{I3} and S_{23}, respectively. To fulfill the above losses condition, either S_{13}, S_{12}, and S_{23} must be equal to zero. Now, three possible combination exist, combination one, $S_{13} = S_{12} = 0$, combination two, $S_{13} = S_{23} = 0$ and combination three $S_{23} = S_{12} = 0$. Substitute these values into Eq. (1) using any of the combinations; it is observed that Eq. (1) is not valid for any of the possible combinations. Therefore, it can be concluded that there is no three-port circulator that can be reciprocal, lossless, and matched simultaneously.

The main aim is to satisfy the design condition where a microwave device will be matched, lossless and non-reciprocal. However, achieving a 100 percent matched or losses microwave device will be difficult. The S matrix for a matched, non-reciprocal and lossless circulator is:

$$[s] = \begin{bmatrix} 0 & s_{12} & s_{13} \\ s_{21} & 0 & s_{23} \\ s_{31} & s_{32} & 0 \end{bmatrix}$$

Applying lossless condition to the s matrix of a three-port circulator, we have

$$S_{31} \times S_{32}^{*} = 0 \quad (3a)$$

$$S_{12} \times S_{13}^{*} = 0 \quad (3b)$$

$$S_{23} \times S_{21}^{*} = 0 \quad (3c)$$

Also, consider unitary case for the 3 port circulator:

$$\left|S_{21}\right|^2 + \left|S_{31}\right|^2 = 1 \quad (4a)$$

$$\left|S_{12}\right|^2 + \left|S_{23}\right|^2 = 1 \quad (4b)$$

$$\left|S_{13}\right|^2 + \left|S_{23}\right|^2 = 1 \quad (4c)$$

To satisfy Eq. 4, S_{31}, S_{12} and S_{23} must be 0. Then, S_{21}, S_{32}, and S_{13} will be 1. In this case, power transfer is from port-1 to port-2, port-2 to port-3 from port-3 to port-1. The s matrix for the clockwise non-reciprocal three-port circulator becomes:

$$[s] = \begin{bmatrix} 0 & 0 & 1 \\ 1 & 0 & 0 \\ 0 & 1 & 0 \end{bmatrix}$$

To realize an anticlockwise, non-reciprocal three-port circulator where power transfers from port-1 to port-3, port 3 to port 2, from port 2 to port 1, S_{13}, S_{21} and S_{32} must be 0. Then, S_{12}, S_{23}, and S_{31} will be 1.

$$[s] = \begin{bmatrix} 0 & 0 & 1 \\ 1 & 0 & 0 \\ 0 & 1 & 0 \end{bmatrix}$$

The three-port diode-based quasi-circulator used for the proposed MOSFET-based absorber antenna has been observed as a clockwise circulator. The performance of the circulator has been analyzed using technical parameters like return loss, reflection coefficient, insertion loss, and VSWR. Firstly, the authors generate the S-parameters of the circulator. To compute the S-parameters, use:

$$S_{11} = \frac{\text{Re } flected\ power\ at\ port\ -\ 1}{incident\ power\ at\ port\ -\ 1} \quad S_{12} = \frac{Transmitted\ power\ to\ port\ -\ 1}{incident\ power\ at\ port\ -\ 2}$$

$$S_{13} = \frac{Transmitted\ power\ to\ port\ -\ 1}{incident\ power\ at\ port\ -\ 3} \quad S_{21} = \frac{Transmitted\ power\ to\ port\ -\ 2}{incident\ power\ at\ port\ -\ 1}$$

$$S_{22} = \frac{\text{Re } flected\ power\ at\ port 2}{incident\ power\ at\ port 2} \quad S_{23} = \frac{Transmitted\ power\ to\ port 2}{incident\ power\ at\ port 3}$$

$$S_{31} = \frac{Transmitted\ power\ to\ port 3}{incident\ power\ at\ port 1} \quad S_{32} = \frac{Transmitted\ power\ to\ port 3}{incident\ power\ at\ port 2}$$

$$S_{33} = \frac{\text{Re } flected\ power\ at\ port\ -\ 3}{incident\ power\ at\ port\ -\ 3}$$

Table II shows *70.559 mW* incident power at port 1 of the circulator. However, in connection with the DMS CSPA, *14.2 mW* power is observed at the input terminal of the DMS CSPA connected to port 2, signifying an *80 %* loss of power. Since *80 %* of power transferred from port 1 to port 2 is lost, *20 %* of power reflected from the antenna branch will be seen at port 3 of the circulator, and the value has been observed as *3.2 mW*, as shown in Table II. Meaning *20 %* of reflected power- from the antenna branch is lost within the circulator.

TABLE II. POWER DESCRIPTION

Power	Transmitted(mW)	Reflected(mW)	Incident(mW)
Port-1	70.559	0	70.559
Port-2	14.2	16	30.4
Port-3	3.2	0	0

To generate the S matrix of the diode-based quasi circulator, substitute values of transmitted, reflected, and incident power at each port into the formula for computing S-parameters of a three-port circulator. Now the S matrix for the diode-based quasi circulator is:

$$[s] = \begin{bmatrix} 0 & 0 & 0 \\ 0.2 & 0.53 & 0 \\ 0 & 0.12 & 0 \end{bmatrix}$$

From the S-matrix, it is observed that the insertion losses S_{21}, S_{13}, and S_{32} are *0.2 (7 dB)*, *0, 0.12 (9.3 dB)*, respectively. The return loss at port-1 (S_{11}), port-2 (S_{22}), and port-3 (S_{33}) have been observed as *0, 0.53 (2.8 dB)* and *0*, respectively. Various microwave devices have different permissible return loss limits; for circulators, antennas,

and other microwave devices, *15 dB* or less is the typical limit [28]. Also, the isolation are equal to zero meaning, $S_{12} = S_{23} = S_{31} = 0$. However, for a practical circulator, S_{12}, S_{23}, and S_{31}, are not equal to zero.

IV. Performance Analysis of MOSFET-Based Absorber ANTENNA Design

Various essential characteristics that impact antenna performance, including resonance frequency, impedance, gain, radiation pattern, polarization, efficiency, and bandwidth, may normally be modified throughout the antenna design process [29]. After simulating the integrated design, return loss, bandwidth resonance frequency, directivity, gain, and efficiency have been used to analyze the antenna's performance in the proposed design.

A. Return Loss, Bandwidth, and Resonance Frequency

The design specifications of an antenna can be altered to improve the return loss. Engineers have adopted different design methodologies to improve return loss value. One of such involves combining a substrate material as presented in [24]. This technique has also been found useful in improving the bandwidth of patch antenna design. Considering the antenna used for the proposed design, a return loss of *-19.22 dB* and *-14.6 dB* have been observed at a resonance frequency of *2.5 GHz* and *5.3 GHz*, respectively, as shown in [25]

A bandwidth of *1 GHz* (*2 GHz to 3 GHz*) and *1.5 GHz* (*4.6 GHz to 6.1 GHz*) has also been recorded for the lower and upper bands, respectively, as shown in ref. [25]. This bandwidth qualifies the proposed integrated design for use in *2.4 GHz* (*2.4 GHz to 2.484 GHz*), *5.2 GHz* (*5.15 GHz to 5.35 GHz)*, and *5.8 GHz* (*5.725 GHz to 5.825 GHz*) WLAN standards, IEEE 802.16 Worldwide Interoperability for Microwave Access (WiMAX) standards of *2.5 GHz* (*2.5 GHz to 2.69 GHz*) and *5.2 GHz* (*5.2 GHz to 5.8 GHz*), and middle band of 5 G

B. Simulated Total Efficiency and Radiation Efficiency

The total simulated efficiency of an antenna takes into account both the losses at the input terminals and the losses within the antenna construction [30]. The predicted fluctuation of total efficiency and radiation efficiency of the antenna utilized for the proposed MOSFET-based absorber antenna with frequency is depicted in Fig. 3.

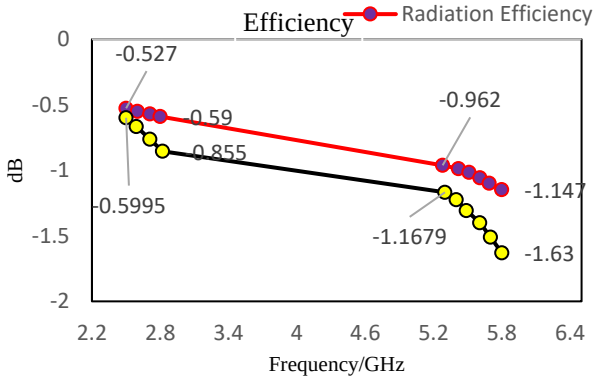

Figure 3. Simulated antenna total efficiency and radiation efficiency plot.

Total efficiency rises from *-0.855 dB* to *-0.5995 dB* (an improvement of *82–87* %) in the lower band region with the resonance frequency of (2.5GHz). Also, when we move from the higher frequency *(6.1 GHz*) to the resonance frequency (*4.6 GHz*), of the upper band region, an improvement in overall efficiency is observed.

C. Insertion Loss and Return Loss of MOSFET-Based Absorber

Engineers utilize total voltage and current measurements to assess any electronic, electrical, or microwave network operation, especially at microwave and millimeter-wave frequencies, when measuring full voltage and current is complex. Scattering parameters are mathematical structures that are used to distribute information [31]. To compute these parameters, the S matrix of the absorber has been generated using the S parameters equation in Section III. Now, Transmitted Power (TP) to port-1 has been calculated using:

$$TP\ to\ port\text{-}1 = RITC \times RITV \tag{5}$$

Here, RITC and RITV stand for the simulated current and voltage at the rectifier's input terminal, respectively. The rectifier input terminal current and voltage are *4.36 mA* and *722 mV*, respectively, as shown in [25]. The reflected power from the circulator incident on port-1 of the absorber is *3.2 mW*. However, at port-2, of the two-port network, the transmitted power to port from port one is computed as follows:

$$TP\ to\ port\text{-}2 = STC \times VDMC \tag{6}$$

Here, STC and VDMC represent simulated source terminal current and the voltage drop across the MOSFET channel, respectively. The source terminal current and voltage drop across the MOSFET channel is *3.6 mA* and *466mV*, respectively, as shown in Table III. When these values are substituted into Eq. (6), the transmitted power to port-2 is *1.677 mW*.

The Incident Power (IP) on port 1 of the two-port network is equal to the transmitted power to port 3 of the circulators and this value is *3.2 mW*, as shown in Table III. To compute reflected power at port-1 and port-2, as:

$$RP\ \text{at}\ port\text{-}1 = IP\ on\ port\text{-}1 - TP\ to\ port\text{-}1 \tag{7}$$

$$RP\ \text{at}\ port\text{-}2 = IP\ on\ port\text{-}2 - TP\ to\ port\text{-}2 \tag{8}$$

The incident power on port 1 and transmitted power to port 1 are equal and the value has been observed *as 3.2 mW*. Therefore, the reflected power at port 1 is zero. For port-2, the incident power on port 2 is *3.2 mW*. Substitute this value into Eq. (8). The reflected power at port-2 has been calculated as *1.5 mW*. Table III shows a summary of power values at each port of the absorber.

TABLE III. Power Values At Each Port of the Absorber

Port	Transmitted(mw)	Reflected(mw)	Incident(mw)
Port 1	3.2	0	3.2
Port 2	1.67	1.5	3.2

Substituting these values into the S parameter equation, S_{11}, S_{12}, S_{21}, and S_{22} have been calculated as 0, 1, 0.53, and 0.47, respectively. Now the S matrix for the MOSFET-based absorber is:

$$[s] = \begin{bmatrix} 0 & 1 \\ 0.53 & 0.47 \end{bmatrix}$$

To compute the insertion loss and return loss of the MOSFET base absorber as:

$$IL_{dB} = 10\log|S_{21}| \tag{9}$$

$$RL_{dB} = 10\log|S_{11}| \tag{10}$$

Engineers formerly used the word attenuation to describe an absorber's absorption, but insertion loss is now the acknowledged standard for describing absorption levels [32]. Here, the insertion loss and return loss were computed as *2.75 dB* and *3.3dB*. This insertion loss value is typical of most absorber materials, which are most helpful at higher GHz frequencies.

D. The Efficiency of MOSFET Base Absorber

Absorbers are designed to provide a volumetric effect, which reduces heat loss and increases absorber efficiency. On the other hand, experiments with volumetric absorbers have not revealed this effect, and the Absorbers' Efficiency is often in the *70% – 80%* range rather than the desired range of over *90%* [33]. Also, absorbers could be designed using metamaterial as presented in [34]. The efficiency of the MOSFET base absorber used for the proposed design was computed as a function of Total Power Absorbed by the MOSFET (TPAM), Total Power Lost in Rectifier (TPLR) circuit, and Reflected Power (RP) from the circulator's port-3. The total power absorbed by MOSFET is equal to the power transmitted to port two of the MOSFET-based absorber; total power loss to the rectifier circuit equals reflected power at port-2 of the two-port MOSFET base absorber. Also, the reflected power from port-3 of the circulator is equal to the power incident on port one of the MOSFET base absorber.

Now the TPAM, TPLR, and RP port-3 are *1.67 mW*, *1.5 mW*, and *3.2 mW*, respectively, as shown in Table III.

To compute the efficiency of the MOSFET-based absorber, use:

$$Eff = \frac{TPAM + TPLR}{RP \text{ port-3}} \times 100 \tag{11}$$

Substituting the values of TPAM, TPLR, and RP port-3 into Eq. (11), the absorber efficiency has been computed as 100 %. A summary of absorber performance parameters is shown in Table IV.

TABLE IV. ABSORBER PERFORMANCE PARAMETER

Reflected power (mW)	Insertion loss (dB)	Return loss (dB)	Efficiency (%)
3.2	2.75	3.3	>90

However, because rectification is part of the RF power absorption process, it may be assumed that the rectifier and MOSFET absorb all reflected power from port-3 of the circulator, and so the model is nearly 100 percent efficient in general. Conclusively, the overall performance of the proposed MOSFET base absorber antenna design is a combination of the performances of individual blocks (double material cylindrical patch antenna, active 3 port circulator, and MOSFET based absorber) used in the proposed design circuitry. Since individual blocks have been observed to have good and acceptable performance characteristics, the proposed MOSFET base absorber antenna design will operate at maximum efficiency.

E. Switching Speed of Proposed MOSFET Base Absorber Antenna

With respect to the proposed model, the switching speed, often referred to as switching time, is expressed as a function of the total time taken for signal transmission from circulator port-1 (directional coupler D_1) to circulator port-2 (directional coupler D_2), Signal reflection from circulator port-2 to circulator port-3 (directional coupler D_3) and signal absorption from circulator port-3 to MOSFET source terminal. Now the switching speed is computed as:

$$T_{Switch} = \Delta T_1 + \Delta T_2 + \Delta T_3 \tag{12}$$

where ΔT_1, ΔT_2, and ΔT_3 are represented as:

$$\Delta T_1 = T_{Port2} - T_{Port1} \tag{13a}$$

$$\Delta T_2 = T_{Port3} - T_{Port2} \tag{13b}$$

$$\Delta T_3 = T_{Drain} - T_{Port3} \tag{13c}$$

where T_{Port1}, T_{Port2}, T_{Port3}, and T_{source} are peak current signal time at port-1, peak current signal time at port-2 peak current signal time at port-3 and current signal time at the drain terminal of MOSFET, respectively.

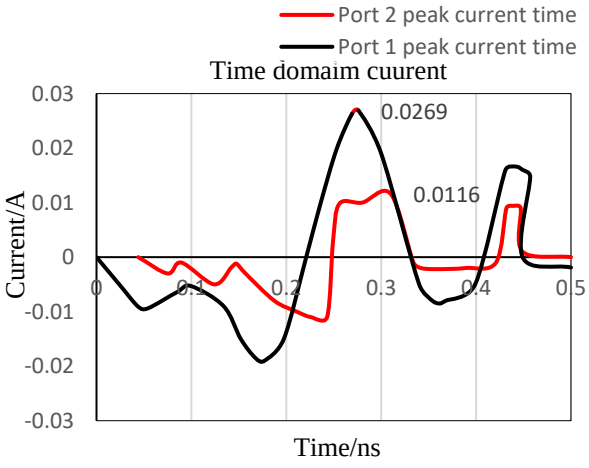

Figure 4. Simulated equivalent signal time at port-1 and port- 2.

From Fig. 4, the peak current signal time at port-1 (T_{Port1}) and peak current signal time at port-2 (T_{Port2}) have been observed as *0.28 ns* and *0.3 ns*, respectively. Substitute

these values into Eq. (13a), ΔT_1 has been calculated as *0.02 ns*. From Fig. 5, the peak current signal time at port-2 (T_{Port2}) and peak current signal time at port-3 (T_{Port3}) have been observed as *0.25 ns* and *0.27 ns*, respectively. Substitute these values into Eq. (13b), ΔT_2 has been calculated as *0.02 ns*.

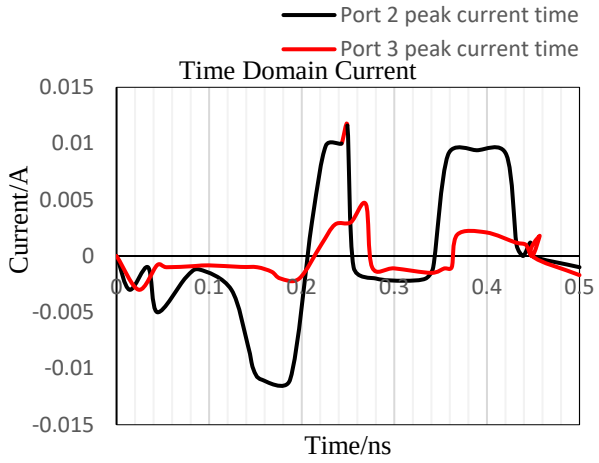

Figure 5. Simulated equivalent signal time at port-2 and port- 3.

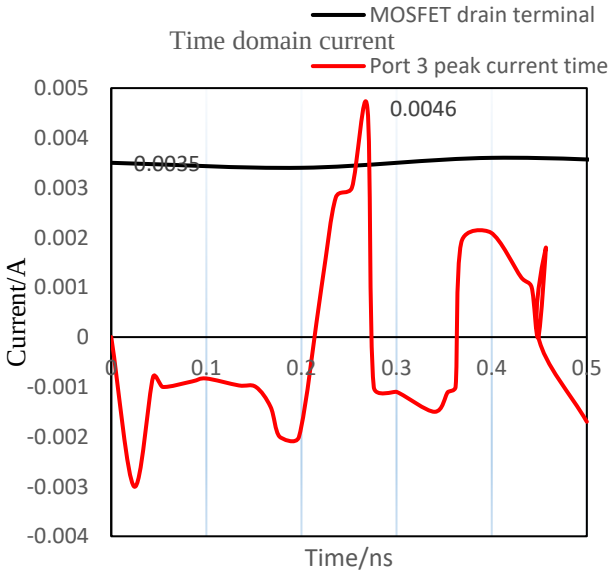

Figure 6. Simulated equivalent signal time at port-3 and signal time at the MOSFET drain terminal.

From Fig. 6, the peak current signal time at port-3 (T_{Port3}) and peak current signal time at the MOSFET drain terminal (T_{Drain}) have been observed as *0.27 ns* and *0.4 ns*, respectively. Substitute these values into Eq. (13c), ΔT_3 has been calculated as *0.13 ns*. Since ΔT_1, ΔT_2, and ΔT_3 have been calculated as *0.02 ns*, *0.02 ns*, and *0.13 ns*, respectively, substitute these values into Eq. (12). Now, the proposed antenna's switching speed or switching time has been calculated as *0.15 ns*.

The possible data rate, spectral efficiency, and capacity of integrated antenna designs are directly impacted by the speed limitations of viable RF switching devices (MOSFET and diode [41-44]) when executing transitions inside antenna-integrated designs. Given that fast data rate is a priority for design engineers in the 5G domain, the proposed MOSFET-based absorber antenna has been shown to have a very good value of switching speed (*0.15 ns*). Due to the absence of previously existing absorber antenna design, the proposed MOSFET-based absorber has been compared with previously existing active antenna designs as shown in Table V.

In Table V, ResF and SwSp stand for resonance frequency and switching speed of the active antenna designs. Comparing this design with previously designed active antenna, the absorber antenna has been observed to have a better return loss value at the lower band frequency compared to the filter antenna in [30, 40].

TABLE V. COMPARISON WITH EXISTING ACTIVE ANTENNA DESIGN

Ref.	Antenna type	ResF (GHz)	SwSp (ns)	Gain (dBi)	Return loss (dB)
[18]	Low noise amplifier	1.57	NA	28	-23.4
[20]	Power amplifier	77	NA	9.4	-14
[21]	Power amplifier	7.1	NA	3.6	<−18
[35]	Low noise amplifier	80	NA	5	-36
[36]	Low noise amplifier	3.9	NA	4.1	-17.5
[37]	Power amplifier	79	NA	15	-I6.5
[38]	Filter	20	NA	2	<−15
[39]	Filter	2.28	NA	NA	-18
[40]	Filter	2.4	NA	4	-17.5
This work	Absorber	2.5/5.3	1.5	2.8/5.8	-26/16

Also, the absorber antenna has been observed to resonate at two frequency bands compared to other forms of active antenna presented in Table V, making it suitable for technologies requiring dual-band operations. The switching speed of the absorber antenna is another noticeable advantage of the absorber antenna.

V. CONCLUSION AND FUTURE WORKS

A new dual-band MOSFET base absorber cylindrical patch antenna has been presented for use in IEEE 802.11, WLAN standard, IEEE 802.16,) and middle band of 5G (*2.3 GHz ~ 2.4 GHz and* 2.5 ~ *2.69 GHz*). The individual performance analysis of each block used in the proposed model circuitry has been used to analyze the overall performance (insertion loss, return loss, gain, directivity, and efficiency) of the MOSFET base absorber antenna and values have been observed to be within acceptable limit. The low directivity value of the presented design makes it suitable for use in mobile devices like phones and laptops.

As a continuation of this work, the authors will present further analysis of the rectifier used for the proposed model circuitry to validate the usability of the proposed 3D circuit co-simulation design in the 5 G regime. In addition, various other MOSFET device structures and various engineering material scan be used [45, 46].

CONFLICT OF INTEREST

The authors declare no conflict of interest.

AUTHOR CONTRIBUTIONS

Elliot. O. Omoru (EOO) done the work for conceptualization, methodology and software. EOO also done the work for validation with Viranjay M. Srivastava (VMS). The formal analysis of this paper was done by EOO; the investigation of this paper was done by EOO and VMS; writing—original draft preparation works were done by EOO; writing—review and editing were done VMS; visualization was done by EOO. All authors had approved the final version.

REFERENCES

[1] H. Zhu, K. Li, J. Lu, and J. Mao, "Millimeter-wave active integrated semi-elliptic CPW slot antenna with ultra-wideband compensation of ball grid array interconnection," *IEEE Transactions on Components, Packaging and Manufacturing Technology*, vol. 12, no. 1, pp. 111-120, Jan. 2022.

[2] W. Lai, "RF front-end CMOS receiver with antenna for millimeter-wave applications," in *Proc. 16th International Conference on Integrated Circuits and Microsystems (ICICM)*, Nanjing, China pp. 332-336, 22-24 Oct. 2021.

[3] R. Kumari, A. Basu, and S. K. Koul, "Frequency reconfigurable high power GaN/AlGaN HEMT based self oscillating active integrated antenna," *Progress in Electromagnetics Research Letters*, vol. 97, pp. 7–12, March 2021.

[4] X.Gu, D. Liu, and B. Sadhu, "Packaging and antenna integration for silicon-based millimeter-wave phased arrays: 5G and beyond," *IEEE Journal of Microwaves*, vol. 1, no. 1, pp. 123-134, Jan. 2021.

[5] A. S. Oluwole and Viranjay M. Srivastava, "Smart antenna for wireless communication systems using spatial signal processing," *Journal of Communications*, vol. 12, no. 6, pp. 328-339, June 2017.

[6] H. Wu and T. Ma "Miniaturized self-oscillating active integrated antenna with quasi-isotropic radiation," *IEEE Transactions on Antennas and Propagation*, vol. 62, no. 2, pp. 933-936, Feb. 2014.

[7] M. Nasrollahpour, A. Romano, M. Zaeimbashi *et al.*, "Integration of a novel CMOS-compatible magnetoelectric antenna with a low-noise amplifier and a tunable input matching," *Analog Integrated Circuits and Signal Processing*, vol. 105, no. 3 pp. 407-415, Oct. 2020.

[8] J. Andrews and P. Hall, "Phase-locked-loop control of active microstrip patch antennas," *IEEE Transactions on Microwave Theory and Techniques*, vol. 50, no. 1, pp. 201-206, Jan. 2002.

[9] D. Singhal and K. Dhwaj, "Dielectric resonator-based evanescent-mode waveguide filtering antenna," *IEEE Antennas and Wireless Propagation Letters* April 2022.

[10] K. Chang, K. Hummer, and L. Klein, "Experiments on injection locking of active antenna elements for active phased arrays and spatial power combiners," *IEEE Transactions on Microwave Theory and Techniques*, vol. 37, no. 7, pp. 1078-1084, July 1989.

[11] Y. Lin and T. Ma, "Frequency-reconfigurable self-oscillating active antenna with gap-loaded ring radiator," *IEEE Antennas and Wireless Propagation Letters*, vol. 12, pp. 337-340, 2013.

[12] K. Bhatt, S. Kumar, P. Kumar and C. C. Tripathi, "Highly efficient 2.4 and 5.8 GHz dual-band rectenna for energy harvesting applications," *IEEE Antennas and Wireless Propagation Letters*, vol. 18, no. 12, pp. 2637-2641, Dec. 2019.

[13] C. Wu and T. Ma, "Pattern-reconfigurable self-oscillating active integrated antenna with frequency agility," *IEEE Transactions on Antennas and Propagation*, vol. 62, no. 12, pp. 5992-5999, Dec. 20.4.

[14] M. Wagih, N. Hillier, S. Yong, A. S. Weddell, and S. Beeby, "RF-powered wearable energy harvesting and storage module based on e-textile co-planar waveguide rectenna and supercapacitor," *IEEE Open Journal of Antennas and Propagation*, vol. 2, pp. 302-314, Feb. 20221.

[15] S. Muhammad, J. J. Tiang, S. K. Wong, A. Smida, R. Ghayoula, and A. Iqbal, "A dual-band ambient energy harvesting rectenna design for wireless power communications," *IEEE Access*, vol. 9, pp. 99944-99953, July 2021.

[16] W. Lai, "RF Transceiver with antenna design for ultra-wideband applications," *IEEE MTT-S International Microwave Filter Workshop (IMFW)*, Perugia, Italy, 17-19 Nov. 2021, pp. 272-274.

[17] B. Kim, J. Jang, C. Kim, and S. Hong, "Integration of SPDT antenna switch with CMOS power amplifier and LNA for FMICW radar front end," *IEEE Transactions on Microwave Theory and Techniques*, vol. 66, no. 11, pp. 5087-5094, Nov. 2018.

[18] D. Rusdiyanto and F. Y. Zulkifli, "Antenna integrated with low noise amplifier operating at L1 GPS application," *IEEE Asia-Pacific Microwave Conference (APMC)*, Singapore, 10-13 Dec. 2019, pp. 1280-1282.

[19] R. Lovato and X. Gong, "A third-order SIW-integrated filter/antenna using two resonant cavities," *IEEE Antennas and Wireless Propagation Letters*, vol. 17, no. 3, pp. 505-508, March 2018.

[20] N. Demirel, Y. Pinto, C. Calvez *et al.*, "Codesign of a PA–antenna block in silicon technology for 80-GHz radar application," *IEEE Transactions on Circuits and Systems II: Express Briefs*, vol. 60, no. 4, pp. 177-181, April 2013.

[21] O. A. Iupikov, J. Cisneros, P. Meye *et al.*, "A cavity-backed patch antenna with distributed multi-port feeding, enabling efficient integration with Doherty power amplifier and band-pass filter," *IEEE Transactions on Antennas and Propagation*, vol. 69, no. 8, pp. 4412-4422, Aug. 2021.

[22] J. Isabona and V. M. Srivastava, "Downlink massive MIMO systems: achievable sum rates and energy efficiency perspective for future 5G systems," *Wireless Personal Communication*, vol. 96, no. 2, pp. 2779-2796, Sept. 2017.

[23] E. Omoru and V. M. Srivastava, "Comparative analysis of dual-band double-material substrate based cylindrical surrounding patch antenna for 5G/WiMAX/WLAN applications," *International Journal on Communications Antenna and Propagation*, vol. 11, no. 6, pp. 430-439, Dec. 2021.

[24] E. O. Omoru and V. M. Srivastava, "Bandwidth and return loss improvement technique using double-material substrate cylindrical surrounding patch antenna: Part-I," *International Journal of Engineering Trends and Technology*, vol. 69, no. 12, pp. 252-256, Dec. 2021.

[25] E. O. Omoru and V. M. Srivastava, "Testing and analysis of MOSFET based absorber integrated antenna for 5G/WiMAX/WLAN applications," *Nanomaterials*, vol. 12, no. 17, article 2911, pp. 1-15, Sept. 2022.

[26] D. Lee, G. Yang, J. Park, and B. Min, "A frequency tunable circulator with 70-dB isolation using reflection coefficient controller for arbitrary load impedance," *IEEE Transactions on Microwave Theory and Techniques*, vol. 69, no. 8, pp. 3797-3803, Aug. 2021.

[27] W. Chen, Z. Deng, Y. Shu, H. J. Qian, and X. Luo, "Low NF and high P1dB wide-band quasi-circulator with unequal power split and reconfigurable inter-stage matching," *IEEE Transactions on Microwave Theory and Techniques*, vol. 69, no. 4, pp. 2241-2252, April 2021.

[28] L. Marzall, S. Verploegh, T. Cappello, M. Roberg, and Z. Popović, "Active MMIC circulator performance in a phased-array-like environment," in *Proc. 50th European Microwave Conference (EuMC)*, Utrecht, Netherlands, pp. 1186-1189, 12-14 January 20.

[29] D. Serghiou, M. Khalily, V. Singh, A. Araghi, and R. Tafazolli, "Sub-6 GHz dual-band 8 × 8 MIMO antenna for 5G smartphones," *IEEE Antennas and Wireless Propagation Letters*, vol. 19, no. 9, pp. 1546-1550, Sept. 2020.

[30] S. Barua, A. Imran, M. Bhuiyan, Z. Rashid, S. A. Gafur, and M. Ahmed, "Highly efficient microstrip patch antenna for wireless gigabit alliance applications," *Indonesian Journal of Electrical Engineering and Computer Science*, vol. 26 no. 3, pp. 1451-1459, June 2022.

[31] Viranjay M. Srivastava, K. S. Yadav, and G. Singh, "Capacitive model and S-parameters of double-pole four-throw double-gate RF CMOS switch," *Int. J. of Wireless Engineering and Technology*, vol. 2, no. 1, pp. 15-22, Jan. 2011.

[32] W. Zhan, J. Xu, and X. Y. Zhang, "Low-loss reconfigurable power divider with arbitrary operating channels using switchable K inverters for antenna feeding network applications," *IEEE Transactions on Microwave Theory and Techniques*, vol. 70, no. 3, pp. 1789-1796, March 2022.

[33] D. Houtz and D. Gu, "A Measurement technique for infrared emissivity of epoxy-based microwave absorbing materials," *IEEE Geoscience and Remote Sensing Letters*, vol. 15, no. 1, pp. 48-52, Jan. 2018.

[34] R. M. O, S. Joseph and R. Ratheesh, "An Efficient Metamaterial Radio Wave Absorber for 2.4GHz ISM band," in *Proc. 3rd IEEE International Conference on Recent Trends in Electronics, Information & Communication Technology (RTEICT*), pp. 648-651

[35] N. Martin, T. Taris, J. B. Begueret, C. Person, and D. Belot, "80 GHz co-designed LNA and antenna for automotive radar," in *Proc. 21st IEEE International Conference on Electronics, Circuits, and Systems (ICECS)*, Marseille, France, 7-10 Dec. 2014, pp. 526-529.

[36] G. M. Roy, S. Dwari, B. K. Kanaujia, S. Kumar, and H. J. Song, "Active feedback supported CMOS LNA blended with coplanar waveguide-fed antenna for Wi-Fi networks," vol. 15, no. 6, pp. 537–546, March 2021.

[37] B. Kim, J. Jang, C. Y. Kim, and S. Hong, "Integration of SPDT antenna switch with CMOS power amplifier and LNA for FMICW radar front end," *IEEE Transactions on Microwave Theory and Techniques*, vol. 66, no. 11, pp. 5087-5094, Nov. 2018.

[38] Z. H. Jiang, F. Wu, T. Yue, and W. Hong, "Wideband and low-profile integrated dual-circularly-polarized transmit-arrays enabled by antenna-filter-antenna phase shifting cells," *IEEE Transactions on Antennas and Propagation*, vol. 69, no. 11, pp. 7462-7475, Nov. 2021.

[39] L. Huitema, Y. Dia, M. Thevenot, S. Bila, A. Perigaud, and C. Delaveaud, "Miniaturization of a filter-antenna device by co-design," *IEEE Open Journal of Antennas and Propagation*, vol. 2, pp. 498-505, Feb. 2021.

[40] Y. Yasir, M. Alkhafaji, H. Alhamadani, N. Parchin, I. Elfergani A. Saleh, J. Rodriguez, and R. Abd-Alhameed, "A new and compact wide-band microstrip filter antenna design for 2.4 GHz ISM Band and 4G applications," *Electronics*, vol. 9, no. 7, pp. 1-13, July 2020.

[41] V. M. Srivastava, K. S. Yadav, and G. Singh, "Double-pole four-throw RF CMOS switch design with double-gate transistors," in *Proc. 2010 Annual IEEE India Council Int. Conference (INDICON)*, India, 17-19 Dec. 2010, pp. 1-4.

[42] V. M. Srivastava, "Relevance of VEE programming for measurement of MOS device parameters," in *Proc. IEEE Int. Advance Computing Conference (IACC)*, India, 6-7 March 2009, pp. 205-209.

[43] A. S. Sedra and K. C. Smith, *Microelectronic Circuits: Theory and Applications*, 7th Ed., Oxford University Press, USA, 2014.

[44] Viranjay M. Srivastava, K. S. Yadav, and G. Singh, "Drain current and noise model of cylindrical surrounding double-gate MOSFET for RF switch," *Procedia Engineering*, vol. 38, pp. 517-521, April 2012.

[45] V. M. Srivastava, "Signal processing for wireless communication MIMO system with nano-scaled CSDG MOSFET based DP4T RF Switch," *Recent Patents on Nanotechnology*, vol. 9, no. 1, pp. 26-32, March 2015.

[46] V. M. Srivastava, "Scaling effect of CSDG MOSFET: A device beyond 22 nm technology," in *Proc. 4th Int. Conf. on Advanced Computing and Communication Systems (ICACCS)*, India 6-7 Jan. 2017, pp. 1-5.